



Baseflow in karst regions is significantly higher than the global average and exhibits spatial variability

Ze Yuan^{1,2}, Qiuwen Zhou^{1,2}, Yuan Li^{1,2}, Yuluan Zhao^{1,2}, and Shengtian Yang^{3,4}

¹School of Geography and Environmental Science, Guizhou Normal University, 550001 Guiyang, China

²Karst Ecosystem Field Scientific Observation and Research Station of Guizhou Normal University & Guanling Autonomous County, 561300 Guanling, China

³Institute of Ecological Civilization, Guizhou Normal University, 550001 Guiyang, China

⁴College of Water Sciences, Beijing Normal University, 100875 Beijing, China

Correspondence: Qiuwen Zhou (zqw@gznu.edu.cn) and Yuan Li (liyuan7pro@163.com)

Received: 15 June 2025 – Discussion started: 28 July 2025

Revised: 22 December 2025 – Accepted: 13 March 2026 – Published: 27 March 2026

Abstract. The distinct hydrogeological configurations of karst terrains engender fundamentally divergent baseflow regimes compared with non-karst systems. However, there is still some uncertainty in the understanding of baseflow in global karst regions due to the variability of methods and differences in natural conditions in different regions. In this study, runoff data from 1375 karst basins around the world were summarized. Graphical and digital filtering methods were employed to estimate the Baseflow Index (BFI, defined as the ratio of baseflow to total streamflow) and to analyze its spatial patterns and trends. The results show that the baseflow index of global karst areas is about $78 \pm 6.9\%$, which is significantly higher than the global average baseflow index (60%). The baseflow index of karst regions in different climatic zones also differed significantly, in which the average baseflow index of arid karst regions (82%) was significantly higher than the average baseflow index of subtropical karst regions (77%). Even within the same climate zone, the baseflow index of different regions may also have significant differences, and the difference of some regions is even $> 10\%$. Vegetation factors reflected in primary productivity have the highest influence on baseflow in karst regions (14.8%), while climatic factors (relative humidity, air temperature, etc.) have a lower influence on BFIs in karst regions (less than 5%). From the time series trend, the global karst baseflow index shows an increasing trend, about 1.5% from 1960 to 2015. These results help us to further understand karst hydrological processes and the response mechanism of karst hydrology under climate change.

1 Introduction

Functioning as a vital component of groundwater recharge to runoff, baseflow acts as a critical hydrological stabiliser (Mukherjee et al., 2018; Chen et al., 2019). The proportion and dynamic characteristics of baseflow in runoff (commonly quantified as the Baseflow Index, BFI) not only regulate the ecological balance threshold of rivers, but also profoundly affect the resilience of watersheds in response to climate fluctuations (Saedi et al., 2022; Hare et al., 2021; Yang et al., 2025). Therefore, accurate quantification of the characteristics of baseflow can help to understand the runoff evolution pattern and its response mechanism to regional environmental changes (Mei et al., 2024; Kuehne et al., 2023).

Recent studies on baseflow estimation have revealed its spatial variability characteristics. Among them, Xie et al. (2024), based on a coupled analysis of baseflow separation and climate models for 15 000 catchments worldwide, pointed out that the average contribution of baseflow to river runoff was about 60%. However, there are significant regional differences under this macroscopic pattern, e.g., baseflow index (BFI) calculations by Beck et al. (2013) for 3394 watersheds globally show that BFI is generally higher in tropical and temperate-cold regions than in arid and semi-arid zones (e.g., North and South Africa, Central Asia, and Australia). Regional-scale studies further refine these spatial patterns. For instance, the BFI is observed to be higher in the eastern regions of both the United States and India compared to their western counterparts (Mei et al., 2024; Sharma

and Mujumdar, 2024). In China, the Yellow River Basin exhibits a 'high-low-high' trend from upstream to downstream, whereas the Wei River Basin shows a gradual decline (Lyu et al., 2023; Zhang et al., 2019).

While current research characterizes general global baseflow features, the distinct hydrogeological architecture of karst landscapes (e.g., conduit and fissure networks) renders these findings significantly less applicable to karst regions (Jing et al., 2024; Ford and Williams, 2007). Observations indicate significant heterogeneity in karst BFI across different climatic zones, which are typically categorized by hydrothermal conditions (e.g., the Köppen classification). In Tropical zones (characterized by high temperature and humidity), the high permeability of karst media facilitates rapid precipitation-to-groundwater conversion; for instance, sub-basins in the Brantas Hulu watershed (Pratama et al., 2020) exhibit BFIs exceeding 80%. Conversely, Arid and Semi-arid regions (defined by water limitation) often show distinct recharge patterns due to scarcity of rainfall. In Subtropical zones, where seasonality is moderate but distinct, baseflow contributions can vary drastically; in central Italy, BFI ranges from 30%–76% annually (Longobardi and Loon, 2018). Similarly, Temperate zones display diverse patterns, such as the Sierra Nevada karst in North America maintaining a BFI above 65% (Tobin and Schwartz, 2020). These disparities highlight the need to consider climatic classification when analyzing global karst hydrology.

In summary, studies of baseflow in karst regions have revealed their obvious spatial heterogeneity. A large number of studies have characterised the baseflow characteristics of karst under different climatic zones, and also outlined the regional baseflow characteristics of karst under different climatic zones (Tagne and Dowling, 2018). However, existing studies still have obvious limitations, starting with an over-focus on localised features in small regions, such as watershed studies in southern China and the Mediterranean (Guisiano et al., 2024; Mo et al., 2021), which makes the results of the study not necessarily representative of the global karst region. The second is the variability of research methods, such as hydrographic methods (graphical methods, digital filtering methods), isotope tracer methods, etc. (He et al., 2019; Yang et al., 2021; Arnold et al., 2012). The difference in focus of the different methods also reduces the commonality of the findings. These two reasons have led to a lack of characterisation of overall features and reasonable quantification of regional differences, despite the exploration of baseflow characteristics of karst basins in different regions of the world (Wu et al., 2017; Mei et al., 2024). Therefore, the complete characterisation of baseflow in the global karst region using reasonable methods and the accurate quantification of the overall characteristics and regional differences of baseflow in the global karst region are still urgently needed.

The overarching aim of this study is to explore the baseflow characteristics and their internal differences across global karst regions, and to evaluate the influence of differ-

ent environmental factors on these characteristics. To achieve this, the following four specific objectives are defined: (i) To evaluate the applicability of twelve baseflow separation methods (including graphical and digital filter methods) in karst watersheds and identify the most suitable approaches. (ii) To reveal the unique hydrological signature of karst baseflow and analyze its spatiotemporal evolution characteristics under changing climate conditions. (iii) To quantify the heterogeneity of baseflow across different karst landform types and clarify the internal differences. (iv) To identify the dominant climatic, topographic, and geological drivers of baseflow variability using an XGBoost machine learning model.

2 Materials and methods

2.1 Data sources

2.1.1 Runoff data

This study focuses on regions with extensive karst landscape distribution globally. By overlaying global watershed boundaries (Lehner and Grill, 2013), Köppen climate zones, and urban distribution maps, we identified candidate runoff observation stations. To minimize anthropogenic disturbance, only watersheds with limited human activity and areas smaller than 2500 km² were selected. Thus daily runoff data for 1412 watersheds with different time spans have been selected. The runoff data mainly comes from the Global Runoff Data Center (<https://www.bafg.de/GRDC>, last access: 20 March 2026), The European Water Archive (https://grdc.bafg.de/data/project_datasets/ewa/index.html, last access: 20 March 2026), National River Flow Archive, UK (<https://nrfaapps.ceh.ac.uk/nrfa/nrfa-api.html>, last access: 20 March 2026), Brazilian National Water Authority (<https://zenodo.org>, last access:), The National Hydrological Data Archive of Canada (<https://wateroffice.ec.gc.ca/>, last access: 20 March 2026), The Chinese Ministry of Water Resources (<http://www.cjh.com.cn/>, last access: 20 March 2026), The National Hydrological Information System of the United States (<https://waterdata.usgs.gov/nwis>, last access: 20 March 2026).

Initially, data from 1412 hydrological stations were compiled. To ensure data quality, a rigorous screening process was applied. Stations with severe data gaps or extensive periods of zero flow were excluded. For stations with minor gaps (less than 30 d), missing values were filled using cubic spline and linear interpolation. This process resulted in a final dataset of 1375 valid karst watersheds covering the period from 1960 to 2015. These watersheds are distributed across different climatic zones, including 221 in tropical, 91 in arid, 490 in subtropical, and 568 in temperate karst regions (Fig. 1).

To ensure consistent climatic characterization, we adopted the Köppen-Geiger climate classification system (Peel et al., 2007) to categorize these watersheds. Specifically, "Tropical

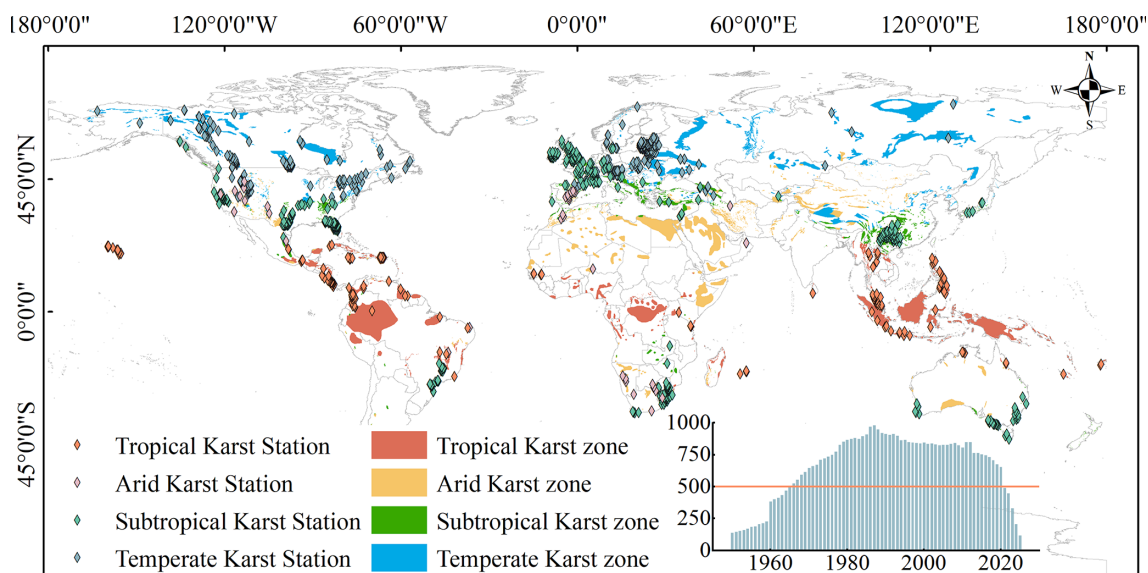


Figure 1. The distribution of karst landscapes and hydrological stations in various climate zones around the world. The bar chart represents the number of hydrological stations selected in each year, with the vertical axis indicating the number of selected hydrological stations and the horizontal axis indicating the year. We selected years with over 500 hydrological stations that meet the requirements within the same year for subsequent analysis.

karst” corresponds to the equatorial zone (Group A), characterized by high temperatures and precipitation year-round. “Arid karst” falls under the arid zone (Group B), defined by water scarcity. “Subtropical karst” primarily includes the warm temperate climates (Group C, e.g., Cfa, Cwa) with hot summers, while “Temperate karst” encompasses the snow climates (Group D) and cool temperate regions (e.g., Cfb), featuring distinct seasonal contrasts and colder winters.

2.1.2 Selection of potential influencing factors of baseflow

In order to analyse the influencing factors of baseflow, we further selected daily-scale runoff data from 744 hydrological stations during 2011–2012 out of the 1375 hydrological stations mentioned earlier to calculate baseflow. The purpose of further selecting the hydrological stations is to ensure the continuity of the data while at the same time ensuring that the stations can cover the major karst regions of the world. We selected a total of 12 potential influences. Climatic factors included temperature and rainfall, and geological factors included depth to bedrock, water storage in epikarst, slope, elevation, and soil evaporation. Other factors included runoff, population density, gross primary productivity (GPP), relative humidity, and surface radiation, for a total of 12 factors (Table 1).

2.2 Methods

2.2.1 Baseflow separation methods

Commonly used methods for baseflow separation include isotope tracer methods, hydrological modeling, and hydrograph analysis (graphical methods and digital filtering). Isotope methods require high-precision data often unavailable in data-scarce regions, while hydrological models are frequently limited by parameter uncertainty and regional applicability.

Given the global scale and data constraints of this study, we selected hydrograph analysis methods for their data efficiency and robustness. We utilized the baseflow Python library developed by Xie et al. (2024) to implement the separation. This tool integrates 12 distinct methods, comprising four graphical methods and eight digital filtering methods. Table 2 provides a detailed summary of the principles and references for each method. For the digital filtering methods, parameter estimation is critical. The recession constant (α) was automatically estimated using the Brutsaert (2008) method. Secondary parameters, where applicable, were calibrated using the multi-objective optimization approach proposed by Arnold (Rammal et al., 2018). The baseflow library automatically evaluates the performance of these methods to determine the optimal separation for each watershed.

Since different methods rely on different assumptions, their performance varies across watersheds. To address this, we employed an optimization strategy provided by the baseflow library. The performance of each method was evaluated by comparing the separated baseflow with the observed

Table 1. Detailed information on the 12 influencing factors.

Name	Temporal scale	Spatial resolution	Data sources
Runoff volume	Monthly average	–	The same as the runoff data in Sect. 2.1.1
Epikarst water storage volume	Monthly average	30 arcsec	GES (Goddard Earth Sciences) DISC (Li et al., 2019)
Bedrock depth	–	0.25 km × 0.25 km	ISRIC – World Soil Information (Hengl et al., 2017)
Air temperature	Monthly average	30 arcsec	Climatic Research Unit gridded Time Series (Harris et al., 2020)
Precipitation	Monthly average	30 arcsec	
Relative humidity	Monthly average	0.1° × 0.1°	
Elevation	–	30 arcsec	Worldclim (Fick and Hijmans, 2017)
Slope steepness	–	30 arcsec	
Available soil moisture	multi-year average	1 km × 1 km	HWSD (Harmonized World Soil Database) (Wieder et al., 2014)
Population density	multi-year average	30 arcsec	LandScan Global 30 Arcsecond Annual Global Gridded Population Datasets (Bright et al., 2013)
Gross primary production	multi-year average	0.25° × 0.25°	TU Data Repository (Wild et al., 2022)
Land-surface radiation	Monthly average	10 km	Data Center of the Qinghai-Tibet Plateau (Tang, 2019)

Table 2. Explanation of 12 Baseflow Separation Methods.

Category	Method (Abbreviation)	Key Principle/Description
Graphical	Fixed Interval (FIM)	Segments hydrograph into fixed intervals; takes minimum flow in each interval as baseflow.
	Local Minimum (LMM)	Identifies local minimum points in the flow time series to demarcate baseflow.
	Sliding Window (SW)	Traverses hydrograph with a fixed-width window, assigning minimum flow to the center point.
	UK Institute of Hydrology (UKIH)	Identifies turning points based on precipitation thresholds and flow response logic.
Digital Filter	Boughton	Single-parameter recursive filter relating current baseflow to previous baseflow and total flow.
	Chapman-Maxwell (CM)	Enhances Chapman filter by dynamically adjusting the recession constant.
	Chapman	Weighted average of current total flow and previous baseflow; corrects constant baseflow issues.
	EWMA	Estimates baseflow by applying exponential weighting to smooth the streamflow series.
	Eckhardt	Two-parameter recursive filter evaluating maximum recession constant and maximum BFI.
	Furey	Based on physical-statistical modeling of hillslope processes using recession constant.
	Lyne-Hollick (LH)	Two-pass filtering process based on signal processing principles.
	Willems	Based on a linear reservoir model and least squares optimization.

streamflow during recession periods (when streamflow is assumed to be purely baseflow). The evaluation metrics included the Nash-Sutcliffe Efficiency (NSE) and Kling-Gupta Efficiency (KGE). For each of the 1375 watersheds, the method yielding the highest evaluation scores was selected as the optimal method for subsequent analysis. This approach minimizes the uncertainty associated with selecting a single arbitrary method for global-scale analysis.

2.2.2 Evaluation metrics for baseflow separation methods

In order to validate the accuracy of different baseflow separation methods in karstic regions, we chose two performance metrics: the KGE and NSE coefficients. Theoretically, these coefficients vary from $-\infty$ to 1; values closer to the maximum of 1 indicate higher accuracy, while values below 0 typically suggest unacceptable performance. The assessment methodology followed Xie et al. (2020), centering on the screening of strict baseflow points to benchmark the separation methods.

The core of screening strict baseflow points lies in excluding periods with precipitation recharge and anomalies in the runoff curve, retaining only the stages where baseflow acts as the primary runoff source. In such stages, there should be a distinct consistency between baseflow and runoff. Therefore, using NSE and KGE coefficients as evaluation criteria can reasonably assess the effectiveness of baseflow separation methods.

2.2.3 Attributional analysis methods

Due to the significant differences in magnitude of the potential influences selected at the global scale (a few hydrological stations are at extremely high elevations, whose actual differences are compressed after normalisation, making it difficult to adequately characterise the effect of elevation on baseflow), traditional linear models or distance metric-based algorithms are susceptible to magnitude interference. Therefore, we chose the magnitude-insensitive XG-Boost model, which naturally circumvents the feature scale difference problem through the splitting rule of the tree structure (Niazkar et al., 2024; Zhang et al., 2023). In addition, the model's built-in regularisation mechanism and subsampling strategy can effectively suppress overfitting and guarantee the model's generalisation ability in complex geographic data. The model also supports parallel computing with automatic processing of missing values, which significantly improves the computational efficiency of large-scale spatial datasets (Chen and Guestrin, 2016).

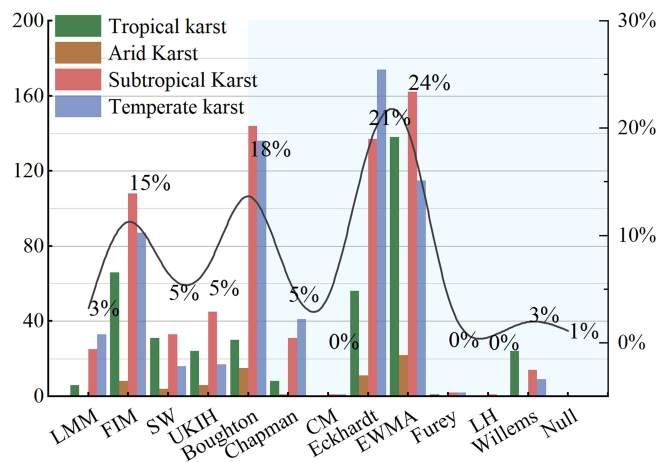


Figure 2. Percentage of best separation methods in the karst region and number of best separation methods in each climatic zone. Graphical methods are shown within the white background, digital filtering methods are shown within the light blue background, and different coloured bars correspond to different climatic zones. The x-axis shows the 12 baseflow separation methods, the y-axis (left) shows the number of hydrological stations, and the y-axis (right) shows the number of hydrological stations covered by each of the optimal baseflow separation methods as a proportion of the number of all hydrological stations, which corresponds to the black curve.

3 Results

3.1 Validation of the applicability of baseflow separation methods

Based on the screening results from the Baseflow library, we identified the optimal baseflow separation method for each hydrological station. As shown in Fig. 2, digital filter methods proved most suitable for the majority of stations (71%), while graphical methods were optimal for 28%. Only 1% of the stations showed no distinct preference for any specific method. Specifically, the Exponential Weighted Moving Average (EWMA) filter emerged as the most effective technique for karst regions, being the optimal choice for 24% of the watersheds. This was followed closely by the Eckhardt filter, which was suitable for 21% of the stations.

Figure 3a illustrates the KGE coefficient distributions for the different baseflow separation methods. Among the digital filtering methods (orange), Boughton, Eckhardt, EWMA, Furey, and Willems exhibit highly concentrated distributions with medians approaching 1, indicating their strong applicability in the karst region. According to the significance analysis (indicated by the letters above the boxplots), EWMA is identified as the optimal method (labeled “a”). Meanwhile, Boughton (“bc”), Eckhardt (“b”), and Willems (“cd”) share overlapping significance groupings, suggesting no statistically obvious disparity in their high performance.

In contrast, the Chapman, CM, and LH methods display highly dispersed distributions with long whiskers extending

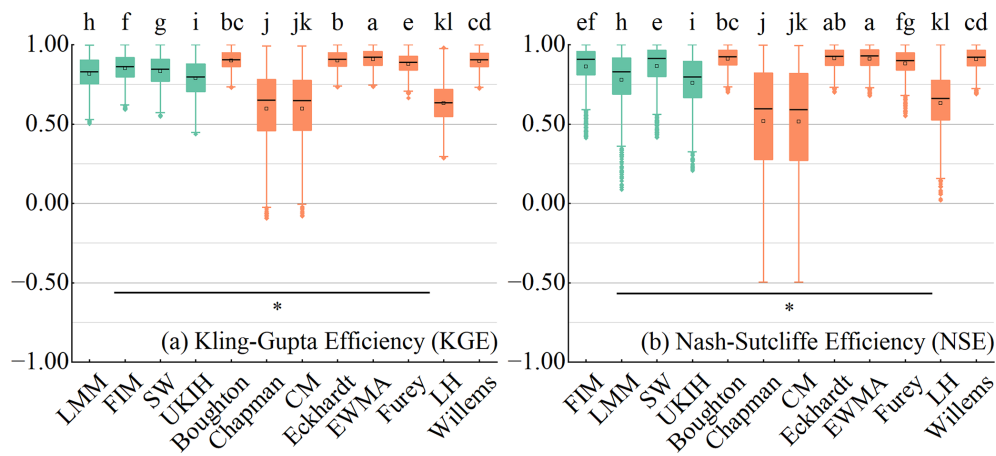


Figure 3. Comparison of KGE coefficients (a) and NSE coefficients (b) for the 12 baseflow separation methods. The x-axis represents each separation method, and the y-axis indicates the value of the coefficients. Green color in the plot denotes the graphical method, while orange denotes the digital filtering method. The letters above the boxes indicate significant differences among the different baseflow separation methods, while the horizontal lines in the lower part of the figure represent significant differences between the graphical method and the digital filtering method. The black line inside the boxplot denotes the mean value, with upper and lower limits set at 1.5 times the interquartile range (IQR). Values exceeding this range are considered outliers and are marked as dots at the top and bottom of the boxplot.

into negative values, indicating significant instability when processing data from different hydrological stations. Despite these fluctuations, the overlapping significance letters (“j”, “jk”, “kl”) confirm there is no significant difference among these three lower-performing methods. For the graphical methods (green), the KGE coefficients are well-distributed (mostly > 0.5), though their letters (“f” through “i”) indicate they statistically rank below the top-tier digital filters. Furthermore, the horizontal line with an asterisk (*) at the bottom signifies a statistically significant difference ($p < 0.05$) between the graphical methods and the digital filtering methods as distinct categories.

The distribution pattern of the NSE coefficients in Fig. 3b mirrors that of Fig. 3a. The EWMA method maintains its status as the optimal sequence (labeled “a”), while Eckhardt (“ab”), Boughton (“bc”), and Willems (“cd”) again form a cluster of high-performing methods with comparable statistical results. The graphical methods show stable distributions with means above 0.5, whereas the Chapman, CM, and LH methods remain highly discrete with wide ranges (-0.5 to 1). Consistent with the KGE results, the significance test in Fig. 3b confirms a significant difference ($p < 0.05$) between the overall performance of graphical methods and digital filtering methods.

From the distribution characteristics of KGE and NSE coefficients in different climatic zones (Fig. 4), it is evident that the distribution patterns of these two coefficients across different zones are generally consistent with the overall coefficient characteristics. Specifically, the KGE coefficients of multiple separation methods in tropical karst have discrete distributions, with CM and Chapman ranging from -1.5 to 1. The NSE coefficients are similar to those of the KGE,

but with a relatively centralised distribution. The distribution of coefficients of graphical methods in the arid karst region are all discrete, and the distribution of KGE coefficients in subtropical and temperate karst is relatively stable and concentrated, and the overall distribution of KGE coefficients of Chapman and CM are also discrete, while the KGE coefficients of FIM and SW are close to 1, which indicates that these methods are more effective in separating the baseflow in subtropical and temperate karst regions.

According to Figs. 2 and 3, considering the high KGE and NSE coefficients and the number of most suitable hydrological stations, we selected four more suitable methods for baseflow separation in karst regions, which are one graphical method (FIM) and three digital filtering methods (Boughton, Eckhardt, EWMA).

3.2 Differences in baseflow indices obtained by different methods over time

From Fig. 5a, it can be found that the four graphical methods have different effects on baseflow separation in karst regions. Among them, the BFIs derived by FIM and SW are similar, with an average value of about 86%. Moreover, the BFI shows an increasing trend of low amplitude with the year, with low fluctuation degree and high stability. The mean value of BFI derived from LMM is about 83%, and the trend of change with years shows a decreasing and then increasing trend, while the result of UKIH method is low, with a mean value of about 77%, and its BFI also shows a slow increasing trend with years.

The results in Fig. 5b can be found that although there are differences in the base flow indices obtained by different digital filtering methods, most of the methods obtain simi-

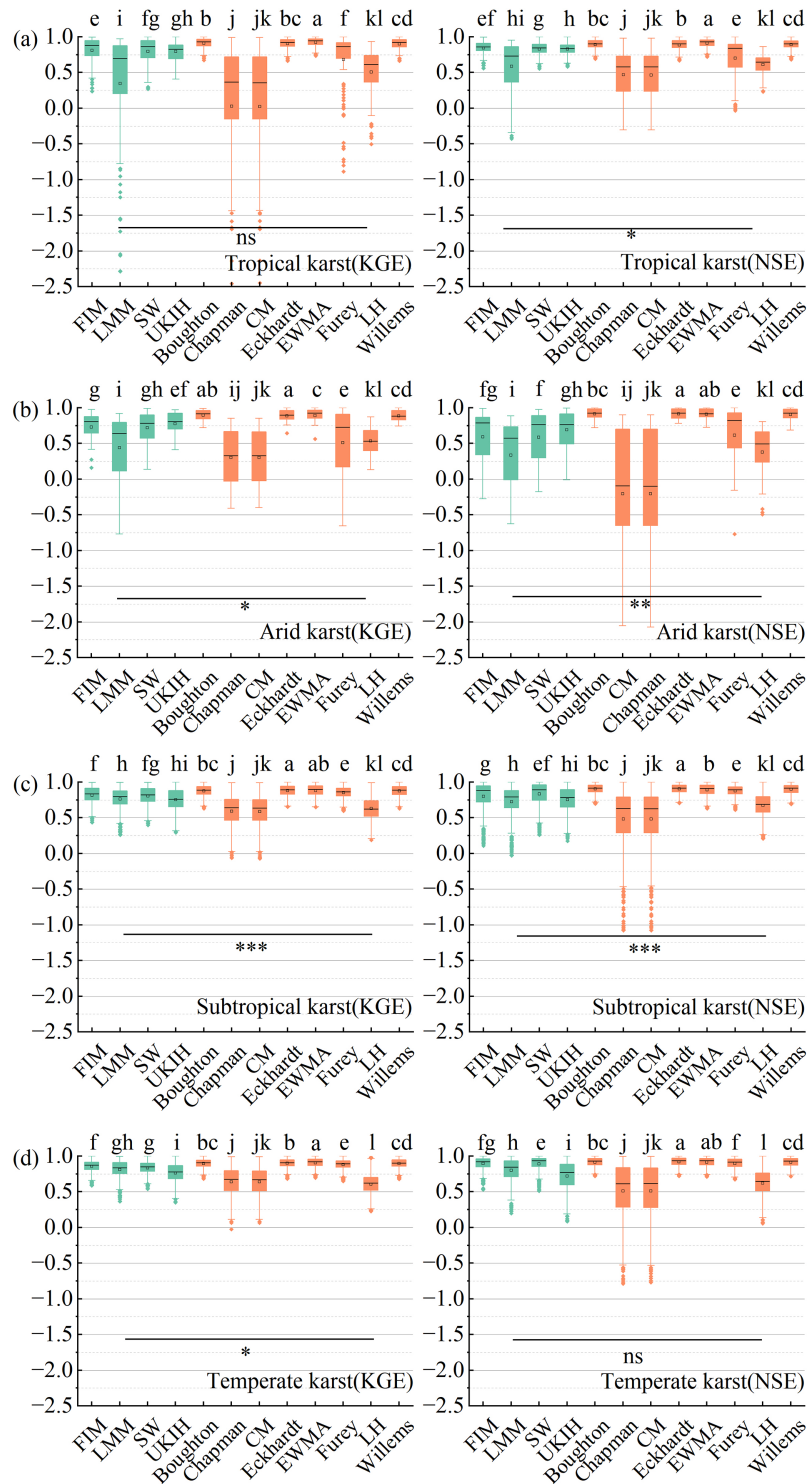


Figure 4. Comparison of KGE coefficients (left) and NSE coefficients (right) for karst regions in different climatic zones (as labeled in the bottom-right corner of each subplot). The x-axis represents each separation method, and the y-axis indicates the coefficient values. The letters above the boxes indicate significant differences among the baseflow separation methods, while the horizontal lines in the lower part of the figure denote significant differences between the graphical and digital filtering method groups. Green color in the plot denotes the graphical method, and orange represents the digital filtering method. The black line inside each boxplot indicates the mean value, with the upper and lower limits set at 1.5 times the interquartile range (IQR). Data points beyond this range are considered outliers and are marked as dots at the top and bottom of the boxplot.

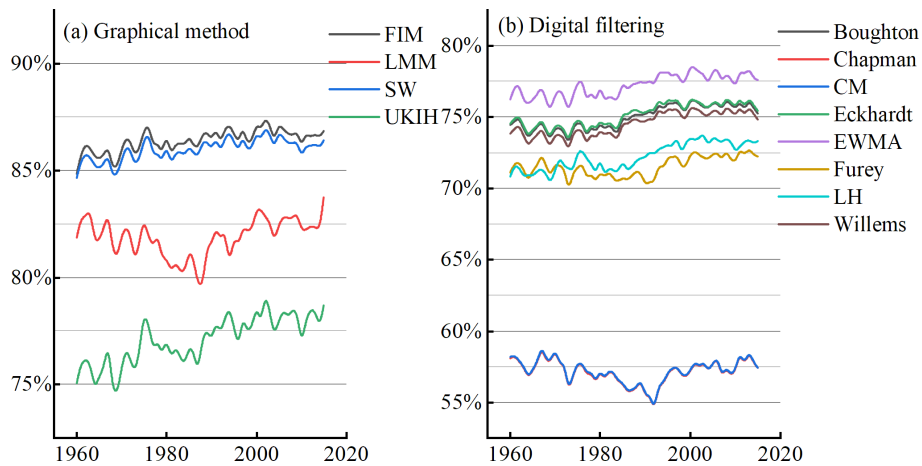


Figure 5. Global BFIs for karst regions calculated by the 12 baseflow separation methods, with the x -axis indicating the year and the y -axis the BFI.

lar base flow indices and have similar trends with respect to year. In contrast, the results of the two methods Chapman and CM differ significantly from those of the other six methods. The mean value of the BFI obtained by the two methods is about 58 %, and there is a small decrease followed by a slow increase in the trend.

In order to analyze the reasons for the differences between these two methods (CM and Chapman) and other methods in separating baseflows, we selected one hydrological station in each climatic zone and generated baseflow curves obtained by the different methods in different climatic zones (Fig. 6). Since the CM method is an improvement of Chapman by adding a maximum baseflow limit to the Chapman method, and its internal mechanism is consistent, Chapman was used as a proxy. In addition, the Eckhardt method with high KGE and NSE coefficients is chosen as a comparison. From Fig. 6, we find that when runoff increases, the Eckhardt method can respond quickly and baseflow increases rapidly, while the Chapman method responds to the increase in runoff to a lesser extent and by a lower amount than Eckhardt. Overall, Chapman responds more slowly to the recharge of precipitation than the other methods, and this feature also makes the Chapman method less discriminating for baseflow compared to the other methods.

3.3 Global base flow characteristics

In order to more clearly characterize the BFI in karst basins, we calculated the BFI in non-karst basins globally using the same method. Figure 7 shows that BFIs in karst basins are significantly higher than in non-karst basins. The BFI of karst basins is 78 ± 6.9 %, while the BFI of non-karst basins is about 60 %. This indicates that baseflow in karst basins is significantly underestimated if only global average conditions are considered and baseflow in karst basins is not calculated separately.

As can be seen from Fig. 7, there are differences in the characteristics of BFIs over time in different climatic zones. The BFI in the tropical karst region generally shows an increasing trend. From 1960 to about 1990, the base flow index in tropical karst showed an increasing trend, and since 1990 the base flow index remained at about 80 % and then stabilized. The BFI in arid karst region is the highest, with a mean value of about 85 %. In general, the BFI in arid karst region shows a decreasing trend, and the annual mean BFI fluctuates greatly, with poor stability. The BFI of subtropical karst region is more stable, always maintained at about 78 %. The characteristics of BFI in temperate karst regions are similar to those of tropical karst, showing a slow increase and remaining stable at around 80 %.

The mean Base Flow Index (BFI) derived from four methods (FIM, Boughton, Eckhardt, and EWMA) was adopted as the BFI for global karst regions. To quantify the trend and its reliability, we calculated the Mann–Kendall test and linear regression metrics (Fig. 8). The analysis reveals a statistically significant increasing trend in BFI ($P = 0.00002 < 0.05$). The model performance metrics – R^2 of 0.62, NSE of 0.825, and KGE of 0.817 – indicate a strong agreement between the fitted trend and observed data, despite natural inter-annual fluctuations. The trend suggests an approximate increase of 1.5 % between 1960 and 2015. A notable rising period occurred from 1980 to 2000. Since 2000, the BFI in global karst regions has stabilized, fluctuating within a range of $78.5 \% \pm 0.5$ %.

Figure 9 shows that, despite being in the same climatic zone, different regions can exhibit differences in BFIs. For example, in the northern part of South America and the Southeast Asian region, which are both tropical Karst, the BFI is significantly higher in the Southeast Asian region (81 %) than in the northern part of South America (73 %). There is also a significant difference in BFIs between the eastern part of the United States and the northern part of

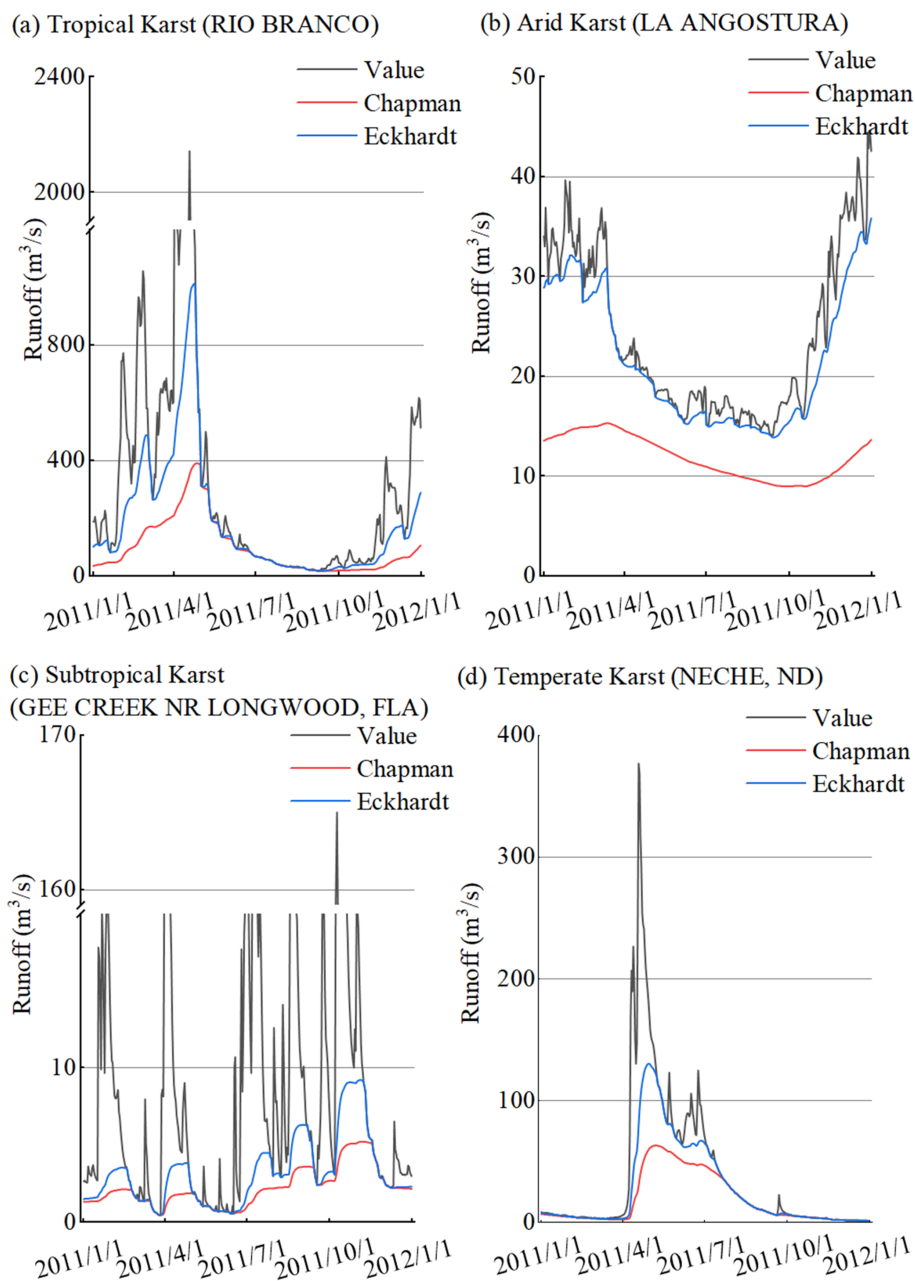


Figure 6. Baseflow curves for different climatic zones (Eckhardt and Chapman methods were chosen as representatives), where the x -axis represents time and the y -axis represents runoff. The black curve (Value) represents the runoff volume. Names of hydrological stations are in parentheses.

Africa, which are both arid karst climate zones. From Figs. 9 and 10 we find that BFI stability is lower and BFI values are higher in arid karst regions. The degree of variation of BFI in tropical karst regions is lower than that in arid karst regions. And subtropical and temperate karst regions have the lowest trend of base flow index change and their stability is higher.

3.4 Factors influencing baseflow indices in karst regions

From a global perspective, runoff volume contributes the most to the Baseflow Index (BFI) in terms of both XGBoost feature importance and SHAP importance (Fig. 11a). The influence of other factors on the BFI remains largely consistent between the two methods. Notably, however, distinct discrepancies exist between the two metrics regarding epikarst

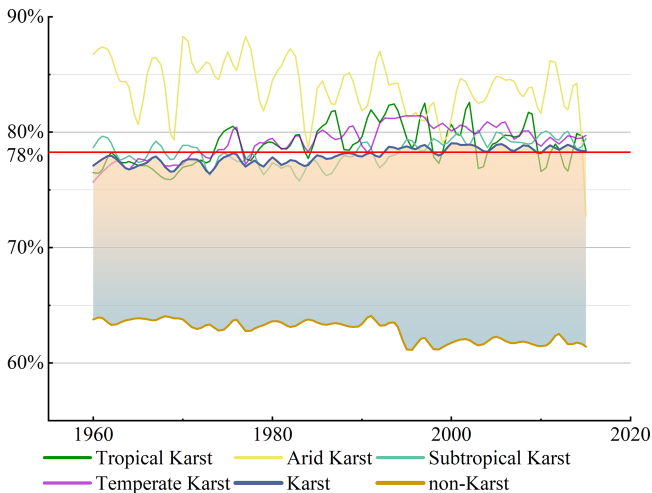


Figure 7. Temporal variations of annual BFI for different karst climatic zones compared to the global average. The x -axis indicates the year, and the y -axis indicates the BFI percentage. The thin colored lines represent the BFI fluctuations in Arid (yellow), Tropical (green), Subtropical (teal), and Temperate (purple) karst regions. The dark blue line represents the weighted average BFI for all karst regions (“Karst”), while the brown curve at the bottom represents the non-Karst average BFI (“non-Karst”). The red horizontal line marks the long-term overall mean of the karst BFI (approximately 78 %).

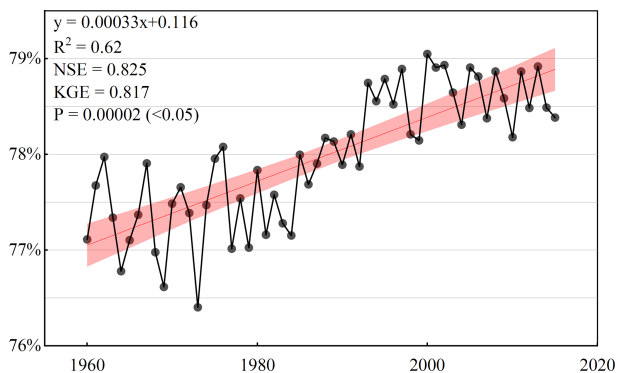


Figure 8. Annual mean BFIs over time for global karst regions. x -axis indicates year, y -axis indicates BFIs, and red bars indicate 95 % confidence interval.

water storage volume and bedrock depth. This is likely because standard XGBoost importance evaluates features from a model-construction perspective (e.g., gain or frequency), whereas SHAP assesses the contribution of features to the specific prediction outcomes.

From a detailed perspective (Fig. 11b), runoff volume and epikarst water storage volume are the most stable positive drivers of baseflow; they exhibit high SHAP values, where larger feature values correspond to a stronger promoting effect. Population density, in contrast, demonstrates a clear inhibitory effect, with high values corresponding to signifi-

cant negative SHAP contributions. Precipitation, serving as a recharge factor, also shows a consistent positive influence. Conversely, the directions of influence for air temperature and land-surface radiation are unstable, suggesting that their effects are highly context-dependent. The remaining topographic and ecological factors have a relatively minor overall impact on baseflow.

4 Discussion

4.1 Mechanisms of formation of baseflow characteristics in karst regions

The results of the study show that the BFI in karst regions is significantly higher than the global average (Fig. 7). We attribute this difference to the unique geological structure and hydrological cycle characteristics of karst regions. Extensively developed fissures, vertical seepage zones, and sub-surface dissolution piping systems in karst regions constitute complex hydrological channels, which significantly alter surface water-groundwater exchange patterns (Ford and Williams, 2007; Li et al., 2024b). Compared with the homogeneous water storage medium dominated by fissures and pores in non-karst areas, the network of dissolution channels in karst regions significantly shortens the infiltration path of precipitation, and its infiltration rate can reach several to tens of times that of in non-karst areas (Fu et al., 2016). For example, the monitoring of karst slopes in Huanjiang, Guangxi, shows that the wet front transport rate is as high as 1373 mm h^{-1} , compared with $17\text{--}610 \text{ mm h}^{-1}$ in non-karst regions, which indicates that the rate of water infiltration in karst regions is much higher than that in non-karst regions (Medici et al., 2019; Zhang et al., 2024). This part of precipitation recharge into the subsurface, under the action of gravity and pressure, squeezes the “old water” out of the underground aquifer, which indirectly enhances the baseflow ratio (Reimann et al., 2011; Bailly-Comte et al., 2010; Evans, 1983; Ronayne, 2013). Studies have shown that this mechanism can result in significantly higher baseflow contributions in karst regions, even above 80 % in specific environments (Zhang et al., 2022), whereas only less than 50 % of precipitation can be converted to baseflow in non-karst regions due to the blocking effect of loose sedimentary layers (Cusano et al., 2024).

Significant differences in surface cover conditions further reinforce baseflow differences. In some karst areas, bedrock exposure exceeds 60 %, and thin layers of residual soil ($< 30 \text{ cm}$) cover only 20 % of the surface, a geologic feature that results in reduced surface interception and elevated subsurface recharge (Anker et al., 2023; Li et al., 2024a; Wang et al., 2024). The karst fissure system is directly exposed to the atmospheric interface, avoiding water loss through evaporation from the soil layer, and the lack of continuous surface cover allows for direct infiltration of large amounts of precipitation (Yang et al., 2025; Li et al., 2023a).

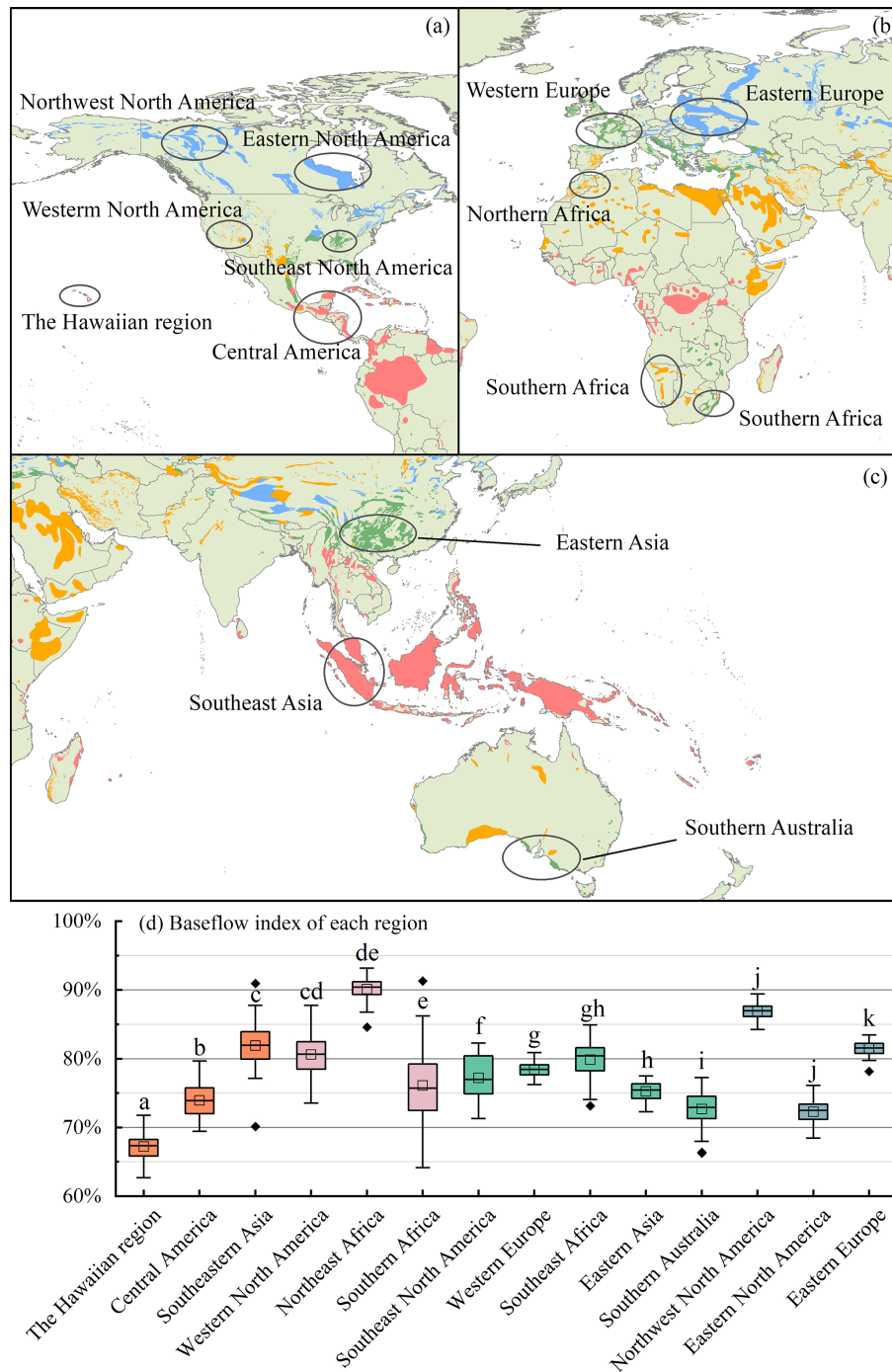


Figure 9. (a–c) Distribution of BFIs in karst basins in different regions within the same climatic zone. In panel (d), orange represents tropical karst regions, magenta represents arid karst regions, green bars represent subtropical karst regions, and brownish-purple represents temperate karst regions.

On the contrary, in non-karst areas, the soil-vegetation system formed by thicker weathered crust constitutes a natural evapotranspiration interface, and the average annual evapotranspiration can reach 40 % of the precipitation, and surface runoff accounts for 30 % of the precipitation, which signifi-

cantly weakened the intensity of groundwater recharge (Jiang et al., 2020; Wang et al., 2020; Wetzel et al., 1996). This double hydrological barrier effect ultimately leads to systematic differences between BFIs in karst regions and non-karst regions.

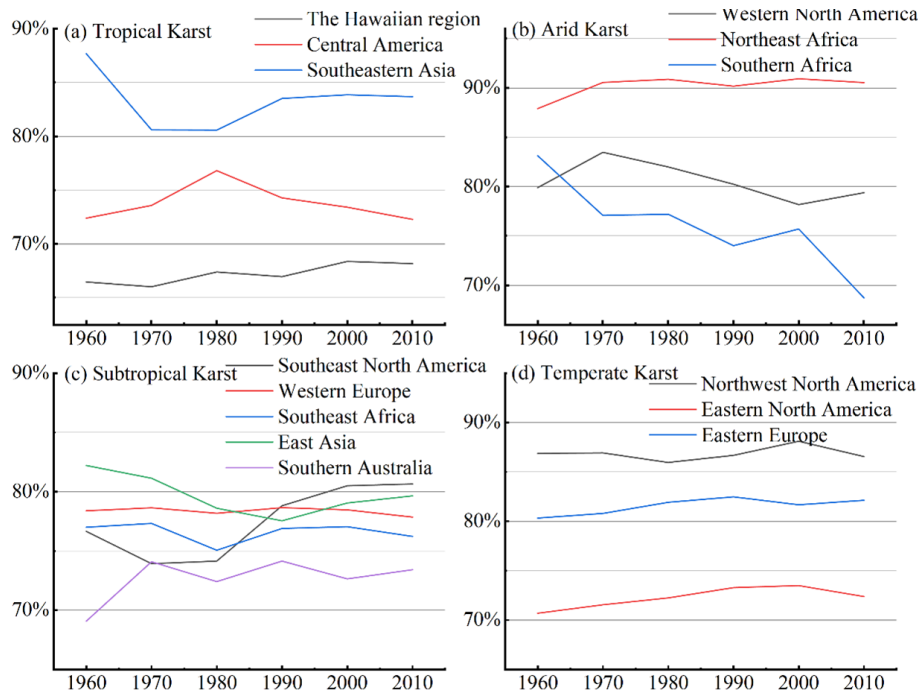


Figure 10. Characteristics of BFIs with respect to year for different regions within the same climatic zone. Where y-axis indicates BFI and x-axis indicates year.

4.2 Reasons for differences in baseflow in karst regions in different climatic zones

The results show that BFIs in karst regions in different climatic zones exhibit significant differences (Figs. 9 and 10). The underlying driving force lies in the heterogeneity of the geologic structure and its coupling effect with long-term climatic erosion (Liu et al., 2023). Among them, the control of the spatial structure of the water storage medium by the geologic context is the decisive factor for the differences in BFIs (Luo et al., 2023). For example, in Southeast Asian karst regions (e.g., Halong Bay, Vietnam), due to the development of high-purity, thick-bedded limestone, and the formation of a pipeline network with vertical dominance under the background of tectonic uplift, the short groundwater runoff paths and efficient recharge mechanisms directly enhance the baseflow (Düringer et al., 2012). In contrast, siliceous interbedding in dolomite formations in northern South America (e.g., Caatinga, Brazil) significantly increases the resistance to dissolution and reduces the connectivity of the dissolution network, a primary geologic feature that fundamentally constrains the baseflow (Teixeira et al., 2023). The intensity of tectonic activity and the stage of geomorphic evolution further strengthen regional differences. For example, strong Cenozoic uplift in Southeast Asia formed steep young landforms that promoted vertical permeability dominance. In contrast, Paleozoic stable landmasses in northern Africa (e.g., the Saharan Atlas Mountains) are dominated by horizontal cave systems, a geologic feature that also distinguishes

the baseflow in this region from that in other regions (Klimchouk, 2007; Jiang et al., 2021). Surface cover characteristics are equally critical as secondary geologic elements. For example, thicker soil layers in temperate zones (e.g., Slovenia) increase surface runoff diversion through delayed infiltration, whereas large areas of exposed bedrock in equatorial zones allow precipitation to infiltrate directly through solution gaps, creating a multiplicative effect on the BFI (Li et al., 2023b).

Climate elements reshape geological structures over large time scales through geological erosion processes, thereby indirectly influencing baseflow patterns. While short-term hydrological dynamics are affected by climate parameters such as precipitation intensity and seasonal distribution (Mo et al., 2025; Cheng et al., 2023), the profound control of climate on the baseflow index is evident in its long-term modification of karst systems. For example, the strong coupling of heavy precipitation and high temperatures in equatorial regions significantly accelerates the dissolution of carbonate rocks, forming a dense network of highly permeable dissolution fissures. Conversely, the persistent moisture associated with temperate maritime climates enhances the dissolution of carbonate rocks (with an average annual dissolution rate approximately 40% higher than that of non-karst areas at the same latitude), leading to the formation of cave clusters characterized by labyrinthine structures and interwoven underground river systems. This climate-driven differentiation in dissolution alters the capacity of groundwater storage spaces, ultimately

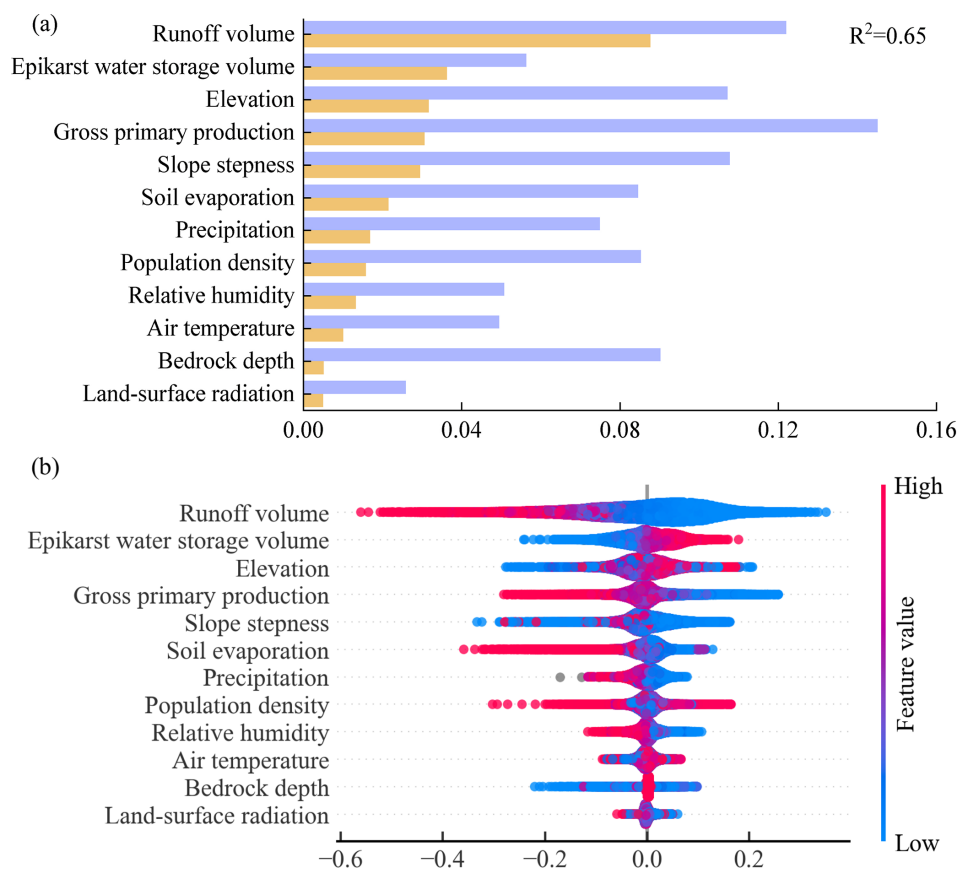


Figure 11. Contribution of different factors to baseflow and their characteristic distributions. Panel (a) illustrates the feature importance derived from XGBOOST and SHAP analysis, with R^2 representing the coefficient of determination of the XGBOOST model. Panel (b) depicts the influence characteristics of various factors on the baseflow index, where the horizontal axis indicates the magnitude of values and the vertical axis lists the different factor types.

being reflected in the characteristic values of regional baseflow indices (Ford and Williams, 2007; Goldscheider, 2015; Tapiador et al., 2012).

4.3 Reasons for changes in baseflow indices over time

The results of the analysis revealed an increasing trend in the BFI in the karst region (Fig. 8). Although the degree of increase is low (about 1.5% from 1960 to 2015), we still consider this degree of increase in BFI noteworthy given that the average BFI in the karst region is already at a high level. This increasing trend in BFI in the karst region is presumably driven by substantial groundwater loss. Extensive monitoring has shown that groundwater levels globally show a rapid declining trend, and this systematic depletion has triggered multiple crises such as basin hydrological process anomalies and regional climate feedback imbalances (Jasechko et al., 2024; de Graaf et al., 2019; Liu et al., 2015). It is the rapid decline of the water table that leads to a constant unsaturated state of groundwater storage. Therefore, when recharged by precipitation, large amounts of precipitation preferentially

replenish the storage deficits, making the generation of surface runoff more difficult and delayed.

In addition to this, the geological and hydrological characteristics of the karst region further amplify this effect of reduced surface runoff and increased baseflow (Zhu et al., 2025). On the one hand, there is the rapid water-conducting effect of the karst fissure network, where the extensive development of dissolution pipes and fissures in the karst bedrock accelerates vertical infiltration of precipitation into deep groundwater, leading to difficulties in retaining soil moisture and a significant increase in the runoff generation threshold (Hartmann et al., 2014). On the other hand, there is the dissipative effect of the surface-subsurface dichotomy, where the thickness of the unsaturated zone of the karst aquifer increases in the context of persistent groundwater overdraft (D’Ettorre et al., 2024), further weakening the immediate contribution of precipitation events to runoff.

4.4 Applicability and limitations of this study

Regarding data sources, the datasets used are inherently diverse and complex. Although substantial efforts were made to exclude studies with distorted data and screen out unreasonable values during calculation, it remains challenging to fully eliminate inherent deficiencies in the original datasets.

There are also limitations regarding the applicability of the methods themselves. For example, the parameterization framework of digital filtering methods (e.g., Eckhardt and Chapman algorithms) based on the assumption of linear recession is at variance with the nonlinear characteristics of karst hydrological processes. Furthermore, the rapid recession processes dominated by karst pipe flow (rates up to 2–3 times those of porous media basins) lead to a general underestimation of the recession coefficient (Kang et al., 2022; Rattayová and Hlavčová, 2023), which leads to differences in baseflow separation between methods with different principles. For instance, the baseflow separation results yielded by the Chapman and CM methods in this study are significantly lower than those of other methods. This discrepancy arises because these methods are less responsive to precipitation recharge, a finding consistent with Helfer et al. (2024). In addition, empirical parameters such as maximum baseflow (BFI_{max}) are mostly derived from calibration results in temperate homogeneous aquifers, and their physical mechanisms have not been fully adapted for applicability in karst regions (Zhou et al., 2017).

Despite the above limitations, this study ensures the spatial representativeness and methodological reliability of the conclusions by integrating a global-scale multi-source dataset of karst regions (covering more than 85 % of the typical karst geomorphological units) and adopting standardized validation indexes (KGE, NSE). The findings demonstrate that the applied baseflow separation techniques can effectively characterize the regional hydrological features and provide data support for water resource management and eco-hydrological model construction in karst regions. Future research can integrate geophysical exploration and isotope tracer technology to develop a dynamic parameterization scheme adapted to non-homogeneous media.

5 Conclusions

This study systematically analyzes the spatial distribution characteristics and trends of BFIs in global karst regions. The results show that the BFI (78 %) in karst regions is generally significantly higher than the global average. This phenomenon confirms the differential regulation of the runoff partitioning mechanism by the unique surface-groundwater dichotomy in karst regions. Meanwhile, the study systematically evaluates the applicability limits of hydrograph separation methods in karst regions and demonstrates their effectiveness. It is noteworthy that the BFI in karst regions shows

a phased upward trend in the context of global groundwater depletion. This may be related to the buffering effect of karst aquifers on extreme climatic events and human activity-induced changes in subsurface storage conditions. Future research should integrate high-precision geological tectonic data and multi-source remote sensing information to construct a coupled climate-hydrology-geology model. This will allow for quantitative analysis of the response characteristics of hydrological fluxes of karst systems in the context of climate change, and further improve the spatiotemporal understanding of the karst water cycle.

Code and data availability. Code and data are publicly available, and access details are provided in the Methods section.

Author contributions. ZY conceived the study, developed the methodology, and wrote the original draft. QZ conducted the formal analysis and investigation and contributed to reviewing and editing the manuscript. YL curated the data and prepared the visualizations. YZ contributed to validation, resources, and project administration. SY supervised the study, acquired funding, and reviewed and edited the manuscript.

Competing interests. The contact author has declared that none of the authors has any competing interests.

Disclaimer. Publisher's note: Copernicus Publications remains neutral with regard to jurisdictional claims made in the text, published maps, institutional affiliations, or any other geographical representation in this paper. The authors bear the ultimate responsibility for providing appropriate place names. Views expressed in the text are those of the authors and do not necessarily reflect the views of the publisher.

Acknowledgements. The authors thank all those who provided valuable assistance during the experimental process.

Financial support. This research has been supported by the National Natural Science Foundation of China (grant nos. 42461004, U1812401, U1612441) and the Science and Technology Program of Guizhou Province (Qiankehejichu-ZK[2025] Zhongdian 045; Qiankehejichu-ZK[2025] Mianshang 268).

Review statement. This paper was edited by Wouter Buytaert and reviewed by Giacomo Medici and one anonymous referee.

References

- Anker, Y., Gimburg, A., Zilberbrand, M., Livshitz, Y., and Mirlas, V.: Groundwater Recharge Assessment for Small karstic Catchment Basins with Different Extents of Anthropogenic Development, *Environments*, 10, 158, <https://doi.org/10.3390/environments10090158>, 2023.
- Arnold, J. G., Moriassi, D. N., Gassman, P. W., Abbaspour, K. C., White, M. J., Srinivasan, R., Santhi, C., Harmel, R. D., van Griensven, A., Van Liew, M. W., Kannan, N., and Jha, M. K.: SWAT: Model Use, Calibration, and Validation, *Trans. ASABE*, 55, 1491–1508, <https://doi.org/10.13031/2013.42256>, 2012.
- Bailly-Comte, V., Martin, J. B., Jourde, H., Sreaton, E. J., Pistre, S., and Langston, A.: Water exchange and pressure transfer between conduits and matrix and their influence on hydrodynamics of two karst aquifers with sinking streams, *J. Hydrol.*, 386, 55–66, <https://doi.org/10.1016/j.jhydrol.2010.03.005>, 2010.
- Beck, H. E., van Dijk, A. I. J. M., Miralles, D. G., de Jeu, R. A. M., Bruijnzeel, L. A., McVicar, T. R., and Schellekens, J.: Global patterns in base flow index and recession based on streamflow observations from 3394 catchments, *Water Resour. Res.*, 49, 7843–7863, <https://doi.org/10.1002/2013WR013918>, 2013.
- Bright, E., Rose, A., and Urban, M.: LandScan Global 2012, Oak Ridge National Laboratory, <https://doi.org/10.48690/1524215>, 2013.
- Brutsaert, W.: Long-term groundwater storage trends estimated from streamflow records: Climatic perspective, *Water Resour. Res.*, 44, W02409, <https://doi.org/10.1029/2007WR006518>, 2008.
- Chen, H., Chen, Y., Li, W., and Li, Z.: Quantifying the contributions of snow/glacier meltwater to river runoff in the Tianshan Mountains, Central Asia, *Global Planet. Change*, 174, 47–57, <https://doi.org/10.1016/j.gloplacha.2019.01.002>, 2019.
- Chen, T. and Guestrin, C.: XGBoost: A Scalable Tree Boosting System, in: *Proceedings of the 22nd ACM SIGKDD International Conference on Knowledge Discovery and Data Mining*, 785–794, <https://doi.org/10.1145/2939672.2939785>, 2016.
- Cheng, S., Yu, X., Li, Z., Xu, X., Gao, H., and Ye, Z.: The effect of climate and vegetation variation on monthly sediment load in a karst watershed, *J. Clean. Prod.*, 382, 135290, <https://doi.org/10.1016/j.jclepro.2022.135290>, 2023.
- Cusano, D., Allocca, V., Coda, S., Di Clemente, E., Fabbrocino, S., Lepore, D., Panza, R., Petrone, P., and De Vita, P.: Effects of ash-fall pyroclastic soil mantle on groundwater recharge of Terminio Mt. peri-volcanic karst aquifer, *J. Hydrol. Reg. Stud.*, 53, 101844, <https://doi.org/10.1016/j.ejrh.2024.101844>, 2024.
- de Graaf, I. E. M., Gleeson, T., van Beek, L. P. H., Sutantudjaja, E. H., and Bierkens, M. F. P.: Environmental flow limits to global groundwater pumping, *Nature*, 574, 90–94, <https://doi.org/10.1038/s41586-019-1594-4>, 2019.
- D’Ettorre, U. S., Liso, I. S., and Parise, M.: Desertification in karst areas: A review, *Earth-Sci. Rev.*, 253, 104786, <https://doi.org/10.1016/j.earscirev.2024.104786>, 2024.
- Duringer, P., Bacon, A.-M., Sayavongkhamdy, T., and Nguyen, T. K. T.: Karst development, breccias history, and mammalian assemblages in Southeast Asia: A brief review, *C. R. Palevol*, 11, 133–157, <https://doi.org/10.1016/j.crpv.2011.07.003>, 2012.
- Evans, G. V.: Tracer techniques in hydrology, *Int. J. Appl. Radiat. Is.*, 34, 451–475, [https://doi.org/10.1016/0020-708X\(83\)90144-8](https://doi.org/10.1016/0020-708X(83)90144-8), 1983.
- Fick, S. E. and Hijmans, R. J.: WorldClim 2: new 1 km spatial resolution climate surfaces for global land areas, *Int. J. Climatol.*, 37, 4302–4315, <https://doi.org/10.1002/joc.5086>, 2017.
- Ford, D. and Williams, P.: *Karst hydrogeology and geomorphology*, John Wiley & Sons Ltd., <https://doi.org/10.1002/9781118684986>, 2007.
- Fu, Z., Chen, H., Xu, Q., Jia, J., Wang, S., and Wang, K.: Role of epikarst in near-surface hydrological processes in a soil mantled subtropical dolomite karst slope: implications of field rainfall simulation experiments, *Hydrol. Process.*, 30, 795–811, <https://doi.org/10.1002/hyp.10650>, 2016.
- Goldscheider, N.: Overview of Methods Applied in Karst Hydrogeology, in: *Karst Aquifers – Characterization and Engineering*, edited by: Stevanović, Z., *Professional Practice in Earth Sciences*, Springer, Cham, https://doi.org/10.1007/978-3-319-12850-4_4, 2015.
- Guisiano, P. A., Santoni, S., Huneau, F., Mattei, A., and Garel, E.: Using natural tracers and calibrated analytical filter to highlight baseflow contribution to mountainous Mediterranean rivers in a context of climate change, *J. Hydrol.*, 641, 131842, <https://doi.org/10.1016/j.jhydrol.2024.131842>, 2024.
- Hare, D. K., Helton, A. M., Johnson, Z. C., Lane, J. W., and Briggs, M. A.: Continental-scale analysis of shallow and deep groundwater contributions to streams, *Nat. Commun.*, 12, 1450, <https://doi.org/10.1038/s41467-021-21651-0>, 2021.
- Harris, I., Osborn, T. J., Jones, P., and Lister, D.: Version 4 of the CRU TS monthly high-resolution gridded multivariate climate dataset, *Sci. Data*, 7, 109, <https://doi.org/10.1038/s41597-020-0453-3>, 2020.
- Hartmann, A., Goldscheider, N., Wägener, T., Lange, J., and Weiler, M.: Karst water resources in a changing world: Review of hydrological modeling approaches, *Rev. Geophys.*, 52, 218–242, <https://doi.org/10.1002/2013RG000443>, 2014.
- He, Z., Unger-Shayesteh, K., Vorogushyn, S., Weise, S. M., Kalashnikova, O., Gafurov, A., Duethmann, D., Barandun, M., and Merz, B.: Constraining hydrological model parameters using water isotopic compositions in a glacierized basin, Central Asia, *J. Hydrol.*, 571, 332–348, <https://doi.org/10.1016/j.jhydrol.2019.01.048>, 2019.
- Helfer, F., Bernardi, F. K., de Barros, C. A. P., Piccilli, D. G. A., Minella, J. P. G., Tassi, R., and Schlesner, A. A.: Calibrated Eckhardt’s filter versus alternative baseflow separation methods: A silica-based approach in a Brazilian catchment, *J. Hydrol.*, 644, 132073, <https://doi.org/10.1016/j.jhydrol.2024.132073>, 2024.
- Hengl, T., Mendes de Jesus, J., Heuvelink, G. B., Ruiperez Gonzalez, M., Kilibarda, M., Blagotić, A., Shangguan, W., Wright, M. N., Geng, X., Bauer-Marschallinger, B., Guevara, M. A., Vargas, R., MacMillan, R. A., Batjes, N. H., Leenaars, J. G., Ribeiro, E., Wheeler, I., Mantel, S., and Kempen, B.: SoilGrids250m: Global gridded soil information based on machine learning, *PLoS one*, 12, e0169748, <https://doi.org/10.1371/journal.pone.0169748>, 2017.
- Jasechko, S., Seybold, H., Perrone, D., Fan, Y., Shamsudduha, M., Taylor, R. G., Fallatah, O., and Kirchner, J. W.: Rapid groundwater decline and some cases of recovery in aquifers globally, *Nature*, 625, 715–721, <https://doi.org/10.1038/s41586-023-06879-8>, 2024.
- Jiang, G., Chen, Z., Siripornpibul, C., Haryono, E., Nguyen, N. X., Oo, T., Manzano, L. S. J., Vongphachanh, S., Kong, S., and

- Guo, F.: The karst water environment in Southeast Asia: characteristics, challenges, and approaches, *Hydrogeol. J.*, 29, 123–135, <https://doi.org/10.1007/s10040-020-02267-y>, 2021.
- Jiang, Z., Liu, H., Wang, H., Peng, J., Meersmans, J., Green, S. M., Quine, T. A., Wu, X., and Song, Z.: Bedrock geochemistry influences vegetation growth by regulating the regolith water holding capacity, *Nat. Commun.*, 11, 2392, <https://doi.org/10.1038/s41467-020-16156-1>, 2020.
- Jing, J., Li, R., Xiao, L., Shu, D., and Yang, P.: Interpreting and modelling the daily extreme sediment events in karst mountain watersheds, *Sci. Total Environ.*, 926, 171956, <https://doi.org/10.1016/j.scitotenv.2024.171956>, 2024.
- Kang, T., Lee, S., Lee, N., and Jin, Y.: Baseflow Separation Using the Digital Filter Method: Review and Sensitivity Analysis, *Water*, 14, 485, <https://doi.org/10.3390/w14030485>, 2022.
- Klimchouk, A. B.: Hypogene speleogenesis: Hydrogeological and Morphogenetic Perspective, NCKRI Special Paper 1, National Cave and Karst Research Institute, Carlsbad, NM, USA, https://digitalcommons.usf.edu/kip_monographs/13 (last access: 16 March 2026), 2007.
- Kuehne, L. M., Dickens, C., Tickner, D., Messenger, M. L., Olden, J. D., O'Brien, G., Lehner, B., and Eriyagama, N.: The future of global river health monitoring, *PLOS Water*, 2, e0000101, <https://doi.org/10.1371/journal.pwat.0000101>, 2023.
- Lehner, B. and Grill, G.: Global river hydrography and network routing: baseline data and new approaches to study the world's large river systems, *Hydrol. Process.*, 27, 2171–2186, <https://doi.org/10.1002/hyp.9740>, 2013.
- Li, B., Rodell, M., Sheffield, J., Wood, E., and Sutanudjaja, E.: Long-term, non-anthropogenic groundwater storage changes simulated by three global-scale hydrological models, *Sci. Rep.*, 9, 10746, <https://doi.org/10.1038/s41598-019-47219-z>, 2019.
- Li, Y., Wang, S., Peng, T., Zhao, G., and Dai, B.: Hydrological characteristics and available water storage of typical karst soil in SW China under different soil–rock structures, *Geoderma*, 438, 116633, <https://doi.org/10.1016/j.geoderma.2023.116633>, 2023a.
- Li, Y., Li, K., Zhou, Q., Zhao, Y., Cai, L., and Yang, Z.: Spatiotemporal dynamics and similarity in soil moisture in shallow soils on karst slopes, *J. Hydrol.*, 639, 131655, <https://doi.org/10.1016/j.jhydrol.2024.131655>, 2024a.
- Li, Y., Zhou, Q., and Zhao, Y.: Hydrologic response in a typical karst desertification catchment, *Carbonate. Evaporite.*, 39, 16, <https://doi.org/10.1007/s13146-024-00929-6>, 2024b.
- Li, Z.-H., Li, S.-T., Du, F., Wang, W.-Q., Li, J.-W., Jiao, Y., and Fan, X.: Research on the development law of karst caves on water conducting fractures under the influence of mining in Southwest karst Mining Areas, *Coal Sci. Technol.*, 51, 106–117, <https://doi.org/10.13199/j.cnki.cst.2023-0409>, 2023b.
- Liu, B., Chen, C., Lian, Y., Chen, J., and Chen, X.: Long-term change of wet and dry climatic conditions in the southwest karst area of China, *Global Planet. Change*, 127, 1–11, <https://doi.org/10.1016/j.gloplacha.2015.01.009>, 2015.
- Liu, X., Fu, Z., Zhang, W., Xiao, S., Chen, H., and Wang, K.: Soluble carbon loss through multiple runoff components in the shallow subsurface of a karst hillslope: Impact of critical zone structure and land use, *CATENA*, 222, 106868, <https://doi.org/10.1016/j.catena.2022.106868>, 2023.
- Longobardi, A. and Van Loon, A. F.: Assessing baseflow index vulnerability to variation in dry spell length for a range of catchment and climate properties, *Hydrol. Process.*, 32, 2496–2509, <https://doi.org/10.1002/hyp.13147>, 2018.
- Luo, Y., Zhou, Q., Peng, D., Yan, W., and Zhao, M.: Key influence of hydrogeological, geochemical, and geological structure factors on runoff characteristics in karst catchments, *J. Hydrol.*, 623, 129852, <https://doi.org/10.1016/j.jhydrol.2023.129852>, 2023.
- Lyu, S., Guo, C., Zhai, Y., Huang, M., Zhang, G., Zhang, Y., Cheng, L., Liu, Q., Zhou, Y., Woods, R., and Zhang, J.: Characterising baseflow signature variability in the Yellow River Basin, *J. Environ. Manage.*, 345, 118565, <https://doi.org/10.1016/j.jenvman.2023.118565>, 2023.
- Medici, G., West, L. J., and Banwart, S. A.: Groundwater flow velocities in a fractured carbonate aquifer-type: Implications for contaminant transport, *J. Contam. Hydrol.*, 222, 1–16, <https://doi.org/10.1016/j.jconhyd.2019.02.001>, 2019.
- Mei, Y., Wang, D., Zhu, J., Tang, G., Cai, C., Shen, X., Hong, Y., and Zhang, X.: Optimal baseflow separation through chemical mass balance: Comparing the usages of two tracers, two concentration estimation methods, and four baseflow filters, *Water Resour. Res.*, 60, e2023WR036386, <https://doi.org/10.1029/2023WR036386>, 2024.
- Mo, C., Ruan, Y., Xiao, X., Lan, H., and Jin, J.: Impact of climate change and human activities on the baseflow in a typical karst basin, Southwest China, *Ecol. Indic.*, 126, 107628, <https://doi.org/10.1016/j.ecolind.2021.107628>, 2021.
- Mo, C., Jiang, C., Long, S., and Cen, W.: Comprehensive evaluation and attribution analysis of baseflow variation in a typical karst basin, Southwest China, *J. Hydrol. Reg. Stud.*, 57, 102185, <https://doi.org/10.1016/j.ejrh.2025.102185>, 2025.
- Mukherjee, A., Bhanja, S. N., and Wada, Y.: Groundwater depletion causing reduction of baseflow triggering Ganges river summer drying, *Sci. Rep.*, 8, 12049, <https://doi.org/10.1038/s41598-018-30246-7>, 2018.
- Niazkar, M., Menapace, A., Brentan, B., Piraei, R., Jimenez, D., Dhawan, P., and Righetti, M.: Applications of XGBoost in water resources engineering: A systematic literature review (Dec 2018–May 2023), *Environ. Model. Softw.*, 174, 105971, <https://doi.org/10.1016/j.envsoft.2024.105971>, 2024.
- Peel, M. C., Finlayson, B. L., and McMahon, T. A.: Updated world map of the Köppen-Geiger climate classification, *Hydrol. Earth Syst. Sci.*, 11, 1633–1644, <https://doi.org/10.5194/hess-11-1633-2007>, 2007.
- Pratama, A. D., Adji, T. N., and Dwiputra, D. S.: Baseflow separation of some springs in the Jonggrangan karst area, Java, Indonesia, *IOP C. Ser. Earth Env.*, 451, 012062, <https://doi.org/10.1088/1755-1315/451/1/012062>, 2020.
- Rammal, M., Archambeau, P., Erpicum, S., Orban, P., Brouyère, S., Piroton, M., and Dewals, B.: Technical note: An operational implementation of recursive digital filter for base flow separation, *Water Resour. Res.*, 54, 8528–8540, <https://doi.org/10.1029/2018WR023351>, 2018.
- Rattayová, V. and Hlavčová, K.: Base flow separation method in conditions of the karst catchment, *Pollack Periodica*, 18, 72–77, 2023.
- Reimann, T., Geyer, T., Shoemaker, W. B., Liedl, R., and Sauter, M.: Effects of dynamically variable saturation and matrix-conduit

- coupling of flow in karst aquifers, *Water Resour. Res.*, 47, W11503, <https://doi.org/10.1029/2011WR010446>, 2011.
- Ronayne, M. J.: Influence of conduit network geometry on solute transport in karst aquifers with a permeable matrix, *Adv. Water Resour.*, 56, 27–34, <https://doi.org/10.1016/j.advwatres.2013.03.002>, 2013.
- Saedi, J., Sharifi, M. R., Saremi, A., and Babazadeh, H.: Assessing the impact of climate change and human activity on streamflow in a semiarid basin using precipitation and baseflow analysis, *Sci. Rep.*, 12, 9228, <https://doi.org/10.1038/s41598-022-13143-y>, 2022.
- Sharma, S. and Mujumdar, P. P.: Spatial synchrony, temporal clustering and dominant driver of streamflow droughts in Peninsular India, *Environ. Res. Lett.*, 19, 074056, <https://doi.org/10.1088/1748-9326/ad53e7>, 2024.
- Tagne, G. V. and Dowling, C.: Inferring groundwater flow and recharge from time series analysis of storm responses in a karst aquifer of southeastern Kentucky (USA), *KIP Articles*, 2659, https://digitalcommons.usf.edu/kip_articles/2659 (last access: 20 March 2026), 2018.
- Tang, W.: Dataset of high-resolution (3 hour, 10 km) global surface solar radiation (1983–2018), National Tibetan Plateau / Third Pole Environment Data Center, <https://doi.org/10.11888/Meteoro.tpd.270112>, 2019.
- Tapiador, F. J., Turk, F. J., Petersen, W., Hou, A. Y., García-Ortega, E., Machado, L. A. T., Angelis, C. F., Salio, P., Kidd, C., Huffman, G. J., and de Castro, M.: Global precipitation measurement: Methods, datasets and applications, *Atmos. Res.*, 104–105, 70–97, <https://doi.org/10.1016/j.atmosres.2011.10.021>, 2012.
- Teixeira, G. M., de Paula, R. S., Velasquez, L. N. M., Andrade, I. B., and Neto, W. M. P.: Evaluation of recharge estimation methods applied to fissure and karst aquifers of the Lagoa Santa karst Environmental Protection Area, Brazil, *Hydrol. Process.*, 37, e14971, <https://doi.org/10.1002/hyp.14971>, 2023.
- Tobin, B. W. and Schwartz, B. F.: Quantifying the role of karstic groundwater in a snowmelt-dominated hydrologic system, *Hydrol. Process.*, 34, 3439–3447, <https://doi.org/10.1002/hyp.13833>, 2020.
- Wang, F., Chen, H., Lian, J., Fu, Z., and Nie, Y.: Hydrological response of karst stream to precipitation variation recognized through the quantitative separation of runoff components, *Sci. Total Environ.*, 748, 142483, <https://doi.org/10.1016/j.scitotenv.2020.142483>, 2020.
- Wang, S., Yan, Y., Zhao, Y., Fu, Z., and Chen, H.: Co-evolution among soil thickness, epikarst weathering degree, and runoff characteristics on a subtropical karst hillslope, *J. Hydrol.*, 628, 130499, <https://doi.org/10.1016/j.jhydrol.2023.130499>, 2024.
- Wetzel, P. J., Liang, X., Irannejad, P., Boone, A., Noilhan, J., Shao, Y., Skelly, C., Xue, Y., and Yang, Z. L.: Modeling vadose zone liquid water fluxes: Infiltration, runoff, drainage, interflow, *Global Planet. Change*, 13, 57–71, [https://doi.org/10.1016/0921-8181\(95\)00037-2](https://doi.org/10.1016/0921-8181(95)00037-2), 1996.
- Wieder, W. R., Boehmert, J., Bonan, G. B., and Langseth, M.: RegridDED Harmonized World Soil Database v1.2, ORNL DAAC [data set], Oak Ridge, Tennessee, USA, <https://doi.org/10.3334/ORNLDAAC/1247>, 2014.
- Wild, B., Teubner, I., Moesinger, L., Zotta, R.-M., Forkel, M., van der Schalie, R., Sitch, S., and Dorigo, W.: VODCA2GPP – a new, global, long-term (1988–2020) gross primary production dataset from microwave remote sensing, *Earth Syst. Sci. Data*, 14, 1063–1085, <https://doi.org/10.5194/essd-14-1063-2022>, 2022.
- Wu, L., Wang, S., Bai, X., Luo, W., Tian, Y., Zeng, C., Luo, G., and He, S.: Quantitative assessment of the impacts of climate change and human activities on runoff change in a typical karst watershed, SW China, *Sci. Total Environ.*, 601–602, 1449–1465, <https://doi.org/10.1016/j.scitotenv.2017.05.288>, 2017.
- Xie, J., Liu, X., Wang, K., Yang, T., Liang, K., and Liu, C.: Evaluation of typical methods for baseflow separation in the contiguous United States, *J. Hydrol.*, 583, 124628, <https://doi.org/10.1016/j.jhydrol.2020.124628>, 2020.
- Xie, J., Liu, X., Jasechko, S., Berghuijs, W. R., Wang, K., Liu, C., Reichstein, M., Jung, M., and Koirala, S.: Majority of global river flow sustained by groundwater, *Nat. Geosci.*, 17, 770–777, <https://doi.org/10.1038/s41561-024-01483-5>, 2024.
- Yang, C., Condon, L. E., and Maxwell, R. M.: Unravelling groundwater–stream connections over the continental United States, *Nat. Water*, 3, 70–79, <https://doi.org/10.1038/s44221-024-00366-8>, 2025.
- Yang, Y., Weng, B., Yan, D., Gong, X., Dai, Y., Niu, Y., and Dong, G.: Tracing potential water sources of the Nagqu River using stable isotopes, *J. Hydrol. Reg. Stud.*, 34, 100807, <https://doi.org/10.1016/j.ejrh.2021.100807>, 2021.
- Zhang, J., Song, J., Cheng, L., Zheng, H., Wang, Y., Huai, B., Sun, W., Qi, S., Zhao, P., Wang, Y., and Li, Q.: Baseflow estimation for catchments in the Loess Plateau, China, *J. Environ. Manage.*, 233, 264–270, <https://doi.org/10.1016/j.jenvman.2018.12.040>, 2019.
- Zhang, J., Wang, S., Fu, Z., Chen, H., and Wang, K.: Soil thickness controls the rainfall–runoff relationship at the karst hillslope critical zone in southwest China, *J. Hydrol.*, 609, 127779, <https://doi.org/10.1016/j.jhydrol.2022.127779>, 2022.
- Zhang, J., Ma, X., Zhang, J., Sun, D., Zhou, X., Mi, C., and Wen, H.: Insights into geospatial heterogeneity of landslide susceptibility based on the SHAP-XGBoost model, *J. Environ. Manage.*, 332, 117357, <https://doi.org/10.1016/j.jenvman.2023.117357>, 2023.
- Zhang, J., Wang, S., Fu, Z., Wang, K., and Chen, H.: Characterizing rapid infiltration processes on complex hillslopes: Insights from soil moisture response to rainfall events, *J. Hydrol.*, 644, 132110, <https://doi.org/10.1016/j.jhydrol.2024.132110>, 2024.
- Zhou, X., Shen, C., Ni, G., and Hu, H.: Digital filter-based baseflow separation method combined with recession curves, *J. Tsinghua Univ.*, 57, 318–330, <https://doi.org/10.16511/j.cnki.qhdxxb.2017.26.016>, 2017.
- Zhu, D.-G., Ning, J., Yang, H., Pu, J.-B., Cao, J.-H., Zhou, M.-X., Prelovšek, M., and Ravbar, N.: Research hotspot and trend of plant water use in karst: Based on a bibliometric analysis from 1984 to 2022, *China Geology*, 8, 214–229, <https://doi.org/10.31035/cg2023134>, 2025.